Absolute measurements of local chromophore concentrations using pulsed photoacoustic spectroscopy

J. Laufer†, C. Elwell, D. Delpy, P. Beard
Department of Medical Physics & Bioengineering, University College London,
Malet Place Engineering Building, London WC1E 6BT, UK

ABSTRACT

Photoacoustic spectroscopy has the potential to make non-invasive, spatially resolved measurements of absolute chromophore concentrations. This has a wide range of possible applications, for example the mapping of endogenous chromophores such as oxy- (HbO_2) and deoxyhaemoglobin (HHb) or externally administered contrast agents designed to target specific tissues or molecular processes. In this study we used near-infrared photoacoustic spectroscopy to determine the absolute concentrations of HbO_2 and HHb in a tissue phantom. The phantom consisted of three blood filled capillaries (Ø460microns) suspended at depths between 3mm and 9mm in a 2.5% Intralipid solution which also contained 2% blood in order to simulate the background optical attenuation in biological tissue. The blood oxygen saturation (SO_2) of the blood circulating in the capillaries was varied using a membrane oxygenator. At each SO_2 level, nanosecond pulses emitted by an OPO laser system that was tuneable over the wavelength range from 740nm to 1040nm illuminated the phantom. The generated photoacoustic waves were recorded using a single Fabry-Perot ultrasound detector and used to obtain a depth profile of the location of the tubes. The amplitudes of the part of the photoacoustic signal that corresponded to the capillaries and the surface of the Intralipid/blood mixture were plotted as a function of wavelength. The output of a diffusion theory based model of the wavelength dependence of the photoacoustic signal amplitude was then fitted to these spectra. This enabled the quantitative determination of absolute HbO_2 and HHb concentrations in the capillaries and the Intralipid/blood mixture from which the total haemoglobin concentrations and blood SO_2 were calculated. Based on these measurements, the smallest chromophore concentrations that can be detected in biological tissue were estimated.

1. INTRODUCTION

Biomedical photoacoustic spectroscopy relies upon the generation of acoustic waves due to the absorption of short optical pulses in tissue. The absorption of the optical energy produces a rapid temperature and subsequent pressure rise resulting in ultrasonic acoustic waves that propagate to the surface of the tissue where they are detected. The amplitude of these waves is directly proportional to the local absorbed energy density, which is dependent upon the distribution of the absorption and scattering coefficients within the illuminated volume. The time history of these waves therefore provides information about the spatial distribution of the absorption coefficient, μ_a, and the scattering coefficient, μ_s. In tissue, the spatial distribution of μ_a is determined by local concentration of the major tissue chromophores of oxyhaemoglobin (HbO_2), deoxyhaemoglobin (HHb), lipids and water. The absorption of each chromophore has a characteristic wavelength dependence, which allows spectroscopic information to be obtained by making photoacoustic measurements at different excitation wavelengths. By analysing the wavelength-dependent photoacoustic response using suitable theoretical models, the local concentrations of these chromophores can be determined. This in turn allows the calculation of physiologically important parameters, such as the oxy- and deoxyhaemoglobin concentrations from which blood oxygen saturation (SO_2) can be calculated [1,2],[3]. Ultimately, by combining photoacoustic spectroscopy with photoacoustic imaging, the technique offers the prospect of providing high resolution quantitative three-dimensional maps of blood SO_2. The technique could also be used to identify and quantify the accumulation of externally administered contrast agents such as those used in molecular imaging applications. In this paper, we report the results of an *in vitro* study aimed at making quantitative, spatially resolved measurements of chromophore concentrations using photoacoustic spectroscopy.

† Correspondence email: jlaufer@medphys.ucl.ac.uk

Photons Plus Ultrasound: Imaging and Sensing 2006: The 7th Conference on Biomedical Thermoacoustics, Optoacoustics, and Acousto-optics, edited by A. A. Oraevsky, et. al
Proc. of SPIE Vol. 6086, 60861J (2006) • 1605-7422/06/$15 • doi: 10.1117/12.657372

2. BACKGROUND

2.1. Photoacoustic signal generation

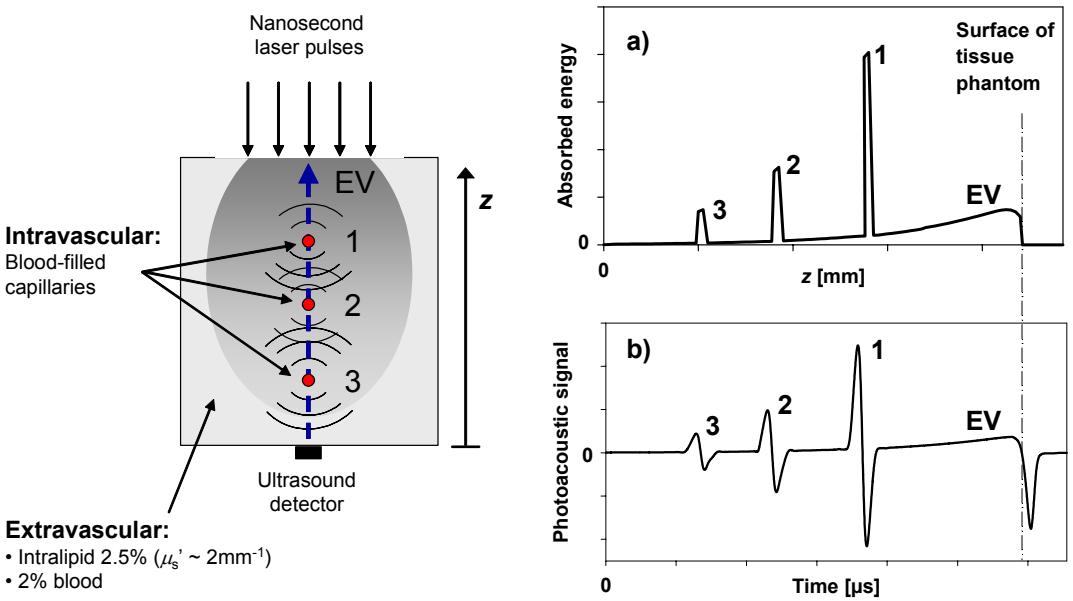

Figure 1. The tissue phantom consisted of a mixture of Intralipid and blood that formed the "extravascular space" (EV) in which three blood-perfused capillaries were suspended. Figure 1(a) shows the depth profile of the absorbed optical energy along the line-of-sight of the ultrasound transducer. Figure 1(b) shows a schematic of the corresponding photoacoustic signal detected in the phantom.

A schematic of the tissue phantom used in this study is shown in Figure 1. The phantom consisted of a mixture of Intralipid and 2% vol. of blood, termed the "extravascular" space, into which three blood-perfused capillaries (termed the "intravascular space") were submerged. Short pulses of near-infrared light irradiated the phantom and the absorption of the optical energy produced acoustic waves that were detected by an ultrasound transducer positioned at the opposite side of the phantom. Under the condition of stress confinement, the time-resolved amplitude of a photoacoustic wave is assumed to be proportional to the absorbed optical energy distribution in the illuminated volume. This is illustrated in Figure 1a and b. Figure 1a shows the distribution of the absorbed optical energy density along the line-of-sight of the ultrasound transducer. The absorbed energy density increases gradually with distance z from the ultrasound transducer whereby the rate of increase is dependent on the optical coefficients of the extravascular space. The increased absorption of haemoglobin results in peaks of absorbed energy where the line-of-sight intersects a blood-filled capillary. The distribution of the absorbed optical energy translates into a photoacoustic signal as shown schematically in Figure 1b. Bipolar waves were generated in the capillaries and at the phantom surface. By plotting the detected photoacoustic signal amplitude corresponding to a particular location in the phantom as a function of the excitation wavelength, spectra that are proportional to the local absorbed energy can be obtained. By fitting a forward model of the wavelength dependence of the photoacoustic signal amplitude, which incorporates the spectral characteristics of the constituent chromophores, to the detected spectrum, the intra- and extravascular concentrations can be determined. The forward model of the wavelength dependent photoacoustic signal amplitude is described in the next section.

2.2. Determination of chromophore concentrations using a forward model of the wavelength dependent photoacoustic signal amplitude

The forward model consisted of a diffusion based finite element model (FEM) of light transport [4] and a model of the acoustic propagation and detection. The FEM calculated the absorbed energy density distribution as a function of the spatial distribution of the optical coefficients across a 2D grid that represented the cross section of the tissue phantom.

The FEM incorporated the delta-Eddington diffusion approximation to ensure that the light transport was modelled accurately in the region close to the optical source [5]. Figure 2 shows an example of the absorbed energy distribution in the phantom calculated by the FEM. The geometric input parameters included the beam diameter, the capillary diameter and the capillary locations, the latter being calculated from the time-of-arrival of the detected photoacoustic waves and the speed of sound in water. The optical input parameters included the scattering coefficient, μ_s, the scattering anisotropy, g, and the absorption coefficients in the extravascular space, μ_{ev}, and in the capillaries, μ_{ai} (where i denotes the number of the capillary). μ_s and g were assumed to be distributed homogenously across the phantom.

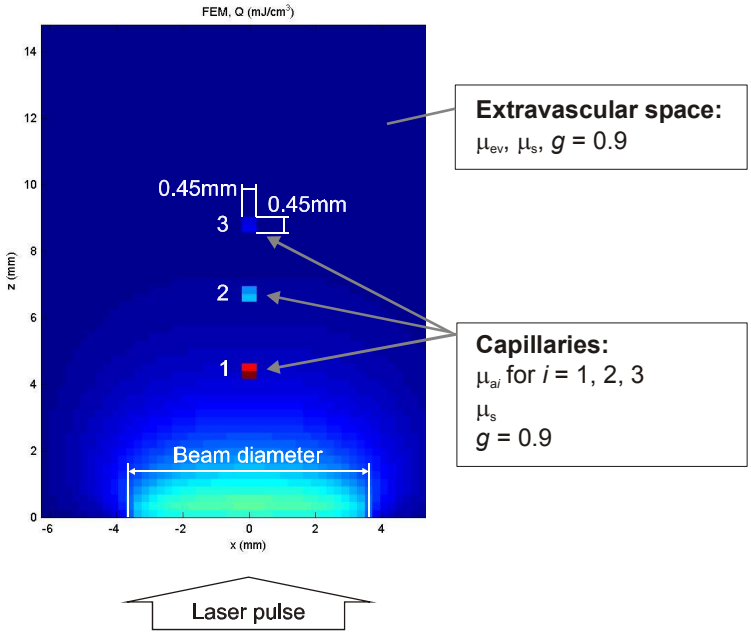

Figure 2 An example of the absorbed energy density distribution in the tissue phantom calculated using the finite element model. The positions of the mesh elements representing the blood vessels were determined from the photoacoustic signal.

The calculated absorbed energy density was converted to an initial pressure distribution using the Grüneisen coefficient. A model of acoustic propagation and detection based on the Poisson integral solution to the wave equation [6] was then used to obtain the theoretical photoacoustic signal amplitude as a function of time t. This model took account of both the directivity of the ultrasound transducer and the attenuation of the photoacoustic waves due to geometrical spreading.

In order to calculate spectra of the photoacoustic signal amplitude using the forward model, the intra- and extravascular absorption coefficients were expressed in terms of the concentrations of the chromophores and their known specific absorption spectra as

$$\mu_{ai}(\lambda) = \alpha_{HHb}(\lambda) c_{HHbi} + \alpha_{HbO_2}(\lambda) c_{HbO_2 i} + \mu_{H_2O}(\lambda) \quad \text{for} \quad i = 1,2,3 \qquad (1)$$

$$\mu_{ev}(\lambda) = \alpha_{HHb}(\lambda) c_{HHbev} + \alpha_{HbO_2}(\lambda) c_{HbO_2 ev} + \mu_{Lipid}(\lambda) + \mu_{H_2O}(\lambda) \qquad (2)$$

where $\alpha_{HHb}(\lambda)$ and $\alpha_{HbO2}(\lambda)$ are the wavelength dependent specific absorption coefficients of deoxyhaemoglobin and oxyhaemoglobin [7], respectively. $\mu_{Lipid}(\lambda)$ represents the wavelength-dependent absorption of the 2.5% volume fraction of lipid [8] in the diluted Intralipid suspension. $\mu_{H2O}(\lambda)$ reflects the absorption of water [9] for a water content in Intralipid of 97.5%. c_{HHbi}, c_{HbO2i} are the deoxy- and oxyhaemoglobin concentrations in the three capillaries (i=1,2,3). c_{HHbev} and c_{HbO2ev} are the concentrations of the extravascular deoxy- and oxyhaemoglobin. Similarly, the scattering coefficient is given as follows

$$\mu_s(\lambda) = \alpha_{scat}(\lambda)\, k_{scat} \qquad (3)$$

where $\alpha_{scat}(\lambda)$ is the wavelength-dependent scattering efficiency and k_{scat} is a scaling factor. $\alpha_{scat}(\lambda)$ was obtained from μ_s spectra measured in Intralipid [10]. The scattering anisotropy factor, g, was assumed independent of wavelength and set to 0.9 for the entire grid of the FEM.

This produced a forward model of the wavelength-dependent photoacoustic amplitude spectra as a function of the intra- and extravascular chromophore concentrations and the scattering coefficient. The known fixed input parameters were $\alpha_{\mathrm{HHb}}(\lambda)$, $\alpha_{\mathrm{HbO2}}(\lambda)$, $\mu_{\mathrm{Lipid}}(\lambda)$, $\mu_{\mathrm{H2O}}(\lambda)$, $\alpha_{\mathrm{scat}}(\lambda)$, the beam diameter, the capillary diameter and the capillary locations. The adjustable unknown input parameters included k_{scat}, $c_{\mathrm{HHb}ev}$, $c_{\mathrm{HbO2}ev}$, $c_{\mathrm{HHb}i}$, $c_{\mathrm{HbO2}i}$ and a scaling factor K. These are varied iteratively until the difference between the measured photoacoustic amplitude spectra and those produced by the forward model is minimised. The values in the adjustable unknown input parameters that were found as a result of the minimisation were regarded as those most likely to represent the true values. Having obtained the oxy- and deoxyhaemoglobin concentrations of the blood in the individual capillaries, other parameters, such as the total intravascular haemoglobin concentration, $c_{\mathrm{THb}i}$, was calculated. This is defined as

$$c_{\mathrm{THb}i} = c_{\mathrm{HHb}i} + c_{\mathrm{HbO_2}i}\,. \qquad (4)$$

The intravascular blood oxygen saturation, SO_2, which is the ratio of the oxyhaemoglobin concentration and the total haemoglobin concentration as given by

$$\mathrm{SO}_{2i} = \frac{c_{\mathrm{HbO_2}i}}{c_{\mathrm{THb}i}}. \qquad (5)$$

The extravascular total haemoglobin concentration was calculated similarly from the determined $c_{\mathrm{HHb}ev}$ and $c_{\mathrm{HbO2}ev}$ values.

3. METHODS

3.1. Experimental set-up

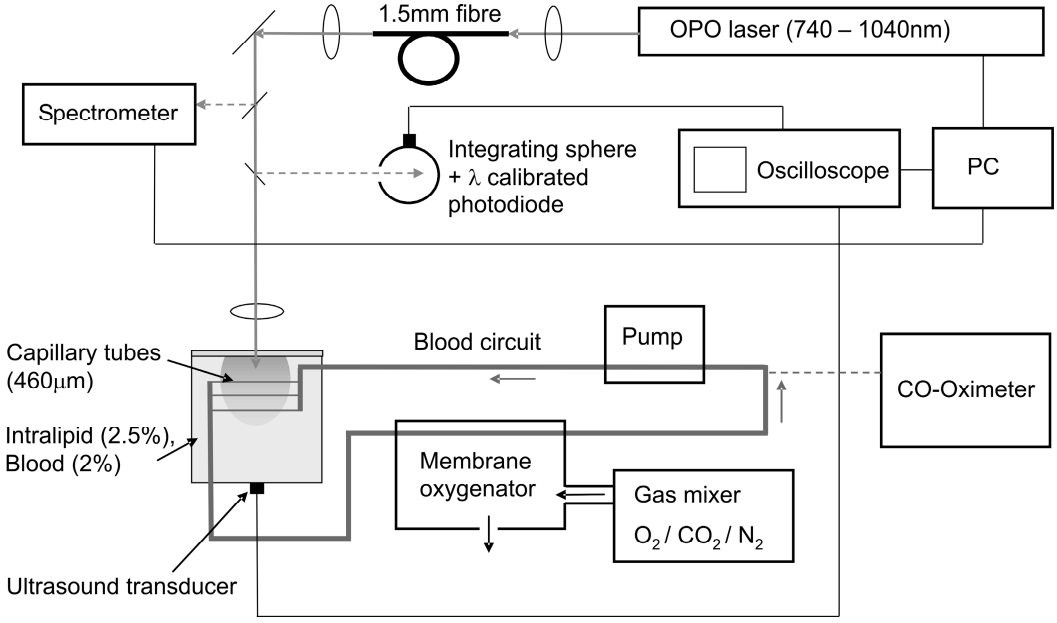

Figure 3 Experimental set-up for the spatially resolved and quantitative measurement of chromophore concentrations in a tissue phantom.

Figure 3 shows the experimental set-up. The tissue phantom consisted of a bath of Intralipid (Fresenius Kabi) with a lipid concentration of 2.5% in which three polymer capillaries (460μm internal diameter, 75μm wall thickness) were suspended at depths of 4.5mm (capillary 1), 6.8mm (capillary 2) and 9.0mm (capillary 3). The Intralipid had an absorption coefficient of 0.05mm^{-1} and a reduced scattering coefficient of 2.0mm^{-1} at 975nm. 2% of blood was added to the Intralipid suspension. The total haemoglobin concentration in the Intralipid ranged between 3.7 and 4.1 g l^{-1}. A saline suspension of red blood cells at physiological haemoglobin concentrations (c_{THb} ~ 150 g l^{-1}) was continuously

circulated through the capillaries and a membrane oxygenator. A gas mixer provided constant flow rates of oxygen, nitrogen and carbon dioxide through the membrane oxygenator and was used to control the intravascular blood SO_2, which ranged from 2% to 100%.

The output of a wavelength-tuneable optical parametric oscillator (OPO) laser system provided 7ns excitation pulses between 740nm and 1040nm, which illuminated the phantom. The beam diameter at the phantom was 7mm and the incident fluence ranged between 40 and 80mJ cm^{-2}. The generated photoacoustic waves were measured using a single detector. Its sensing mechanism is based on acoustically induced changes in the optical thickness of a 75μm thick Fabry-Perot polymer film interferometer and provides broadband (15MHz) detection sensitivity of 0.5kPa noise equivalent pressure [11]. The OPO wavelength was measured using a spectrometer (EPP2000, StellarNet Inc) with a resolution of 0.3nm. Another portion of the incident light was directed onto an integrating sphere and measured with a wavelength-calibrated photodiode in order to normalise the photoacoustic waveforms with respect to the incident pulse energy. The photodiode output and the photoacoustic waveforms were captured and averaged over 60 acquisitions using a digital oscilloscope (TDS743D, Tektronix). The acquisition was repeated three times for each wavelength. The wavelength scans were made between 740nm and 1100nm in 10nm steps.

Wavelength scans were made at different intravascular blood SO_2 levels. Small samples of blood were taken from the intravascular circuit at several times during the wavelength scan. The samples were analysed using a CO-oximeter (IL482, Instrumentation Labs Inc), which provided gold standard measurements of the total haemoglobin concentration (±3.0 g l^{-1}), the haemoglobin fractions %HbO_2 (±1%) and %HHb (±3%), and SO_2 (±4.1%) against which the photoacoustically measured haemoglobin concentrations and SO_2 could be compared.

3.2. Extraction of photoacoustic spectra

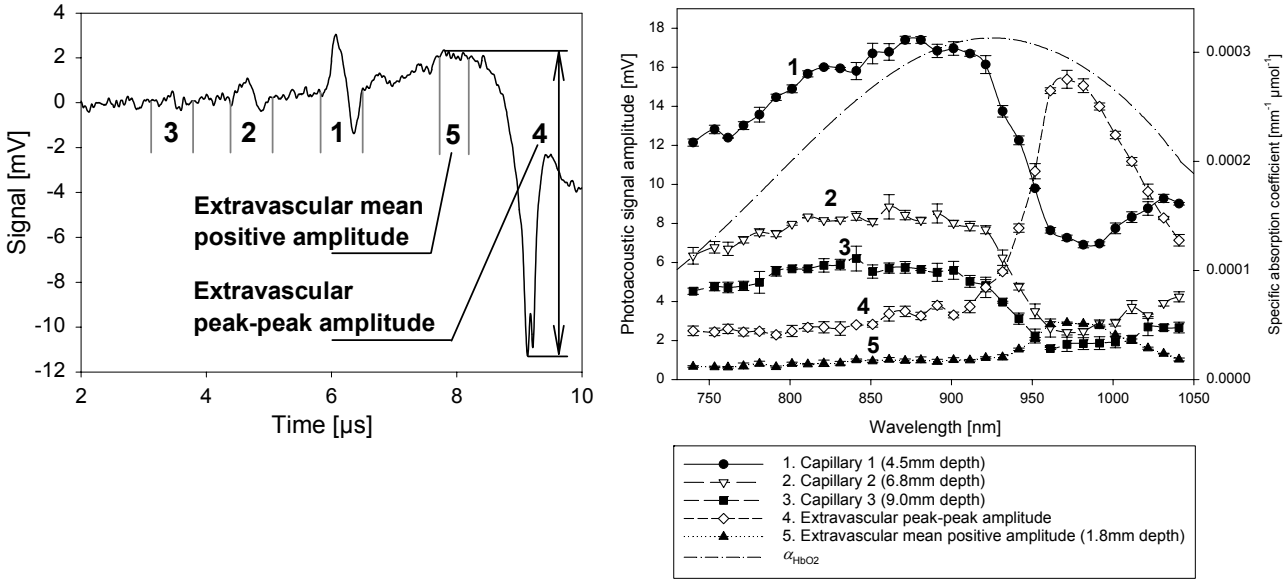

Figure 4 The left hand graph shows a typical photoacoustic signal detected at λ=975nm and indicates the parts of the signal from which the spectra were obtained. The right hand graph shows examples of photoacoustic spectra, which were extracted from the sections of the detected photoacoustic signal that corresponded to the locations of the capillaries and the extravascular space of the tissue phantom as indicated by the numbers. In this example, the blood SO_2 in the capillaries was 93%. The spectrum of the specific absorption coefficient, α_{HbO2}, of oxyhaemoglobin, which is shown for comparison, is very different to the photoacoustic spectra, which are affected by the wavelength-dependent optical attenuation in the extravascular medium.

Figure 4 shows examples of photoacoustic spectra detected in the tissue phantom. The left hand graph in Figure 4 shows a typical photoacoustic signal and indicates the sections from which the photoacoustic spectra were extracted. The sections marked 1 to 3 corresponded to the locations of the capillaries. Two spectra, which are marked 4 and 5 were

extracted from the extravascular part of the photoacoustic signal. Spectrum 4 is the peak-peak amplitude and spectrum 5 is the mean positive amplitude of the signal from the phantom surface as a function of wavelength.

The capillary spectra shown in Figure 4 were detected in blood that was highly oxygenated. In standard spectroscopy, a linear model ($\mu_a = \Sigma \alpha_i \, c_i$) would be used to obtain blood SO_2 and chromophore concentrations from the measured spectra. This model assumes that the photoacoustic signal amplitude is directly proportional to the absorption coefficient, which can be expressed in terms of the chromophore concentrations. For the case of the measurements shown in Figure 4, this would imply that the photoacoustic spectra corresponding to the capillaries are proportional to the specific absorption coefficient spectrum of oxyhaemoglobin, which is shown for comparison. The α_{HbO2} spectrum does not agree with the measured data because the photoacoustic signal amplitude is proportional to the local absorbed energy density, which itself is not a linear function of μ_a. This underlines the importance of using a suitable model of light transport for the analysis of photoacoustic amplitude spectra if accurate quantitative results are to be obtained.

4. RESULTS

The Bland-Altman plots in Figure 5 show the percentage difference, ΔPA c_{THb1}, between the photoacoustically determined intravascular total haemoglobin concentration, PA c_{THb1} (capillary 1), and that measured using the CO-oximeter. ΔPA c_{THbi} was obtained using

$$\Delta \,\mathrm{PA}\, c_{\mathrm{THb}i} = \frac{\mathrm{PA}\; c_{\mathrm{THb}i}}{\mathrm{CO-oximeter}\; c_{\mathrm{THb}i}} \times 100\% \; - 100\% . \qquad (6)$$

The accuracy in the photoacoustic c_{THb1} is equal to the mean of all data points shown in Figure 5, which was found to be +8.1%. The standard deviation of the data points, which was ±16.6%, provides a measure of the precision of the technique. The error bars indicate the uncertainty in the determined values and are a result of experimental error sources such as signal noise. The average of the uncertainties in the determined concentrations is therefore equivalent to the resolution of the technique, which was ±5.3 g l^{-1} for the results shown in Figure 5.

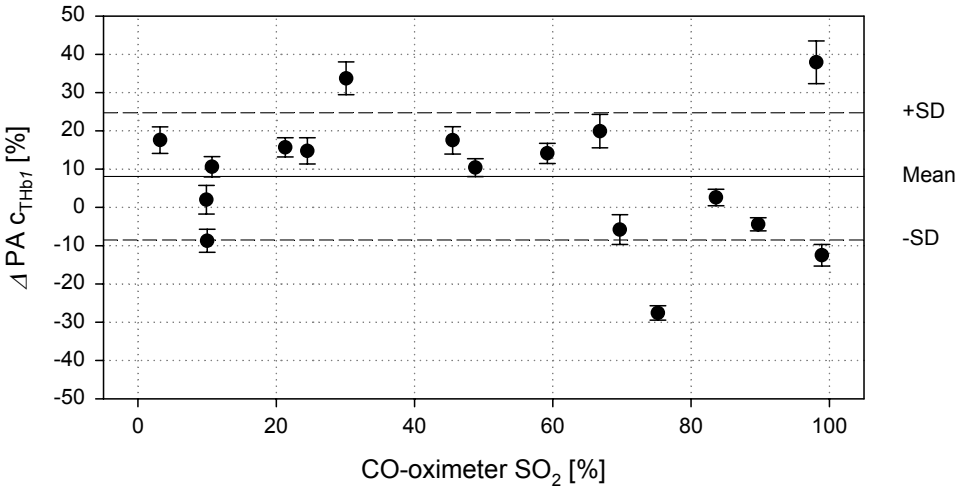

Figure 5 Bland-Altman plots of the accuracy of the photoacoustically determined total haemoglobin concentration in capillary 1 compared to the CO-oximeter measurements. The error bars represent the uncertainties in the determined c_{THb1} values. The mean value of the data is equivalent to the accuracy of the technique while the standard deviation (SD) provides a measure of its precision.

The determined intravascular oxy- and deoxyhaemoglobin concentrations allowed the calculation of blood SO_2 using equation (6). The deviation of the photoacoustically determined values compared to the CO-oximeter measurements together with the accuracy (mean = -3.7%SO_2) and precision (SD = ±4.2%SO_2) is shown in Figure 6. The blood SO_2 resolution was calculated from the error bars as ±2.8%SO_2. The analysis described in the previous two paragraphs was also applied to capillary 2 and 3. The results are shown in Table 1.

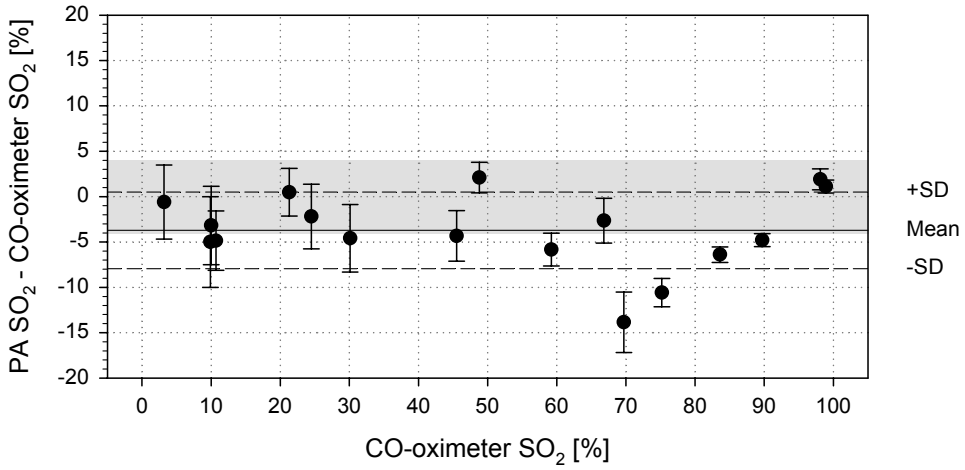

Figure 6 Bland-Altman plots of the accuracy of the photoacoustically determined blood SO_2 measurements in capillary 1 compared to the CO-oximeter measurements. The error bars represent the uncertainties in the determined SO_2 values. The average of the uncertainties provides a measure of the resolution of the photoacoustic blood SO_2 measurements. The grey bar indicates the uncertainty in the CO-oximeter measurements, which was ±4.1%.

	c_{THbi} accuracy [%]	c_{THbi} resolution [g l^{-1}]	%SO_2 accuracy	%SO_2 resolution
Capillary 1 (4.5mm depth)	+8.1 ± 16.6	±5.3	-3.7 ± 4.2	±2.8
Capillary 2 (6.9mm depth)	-16.0 ± 13.5	±6.4	-0.5 ± 5.9	±4.3
Capillary 3 (8.8mm depth)	-25.0 ± 16.8	±7.5	+7.0 ± 11.0	±5.7

Table 1 Accuracy and resolution in c_{THbi} and blood SO_2 obtained using photoacoustic spectroscopy. The accuracy in the photoacoustic c_{THBi} is given as the percentage deviation from the CO-oximeter c_{THb}.

The accuracy in c_{THbi} shows systematic errors with an overreading for capillary 1 that changes into an underreading for capillary 3. This is most likely due to the limitations of the forward model. For example, relatively small inaccuracies in the prediction of the directivity of the acoustic detector would result in errors in the determined extravascular haemoglobin concentration, which would in turn produce errors in the intravascular c_{THbi}. The resolution in c_{THbi} was found to decrease with increasing capillary depth, which was due to the associated reduction in the signal-to-noise ratio. The accuracy, precision and resolution in SO_2 for capillary 1 and 2 shown in Table 1 is comparable to that of the CO-oximeter. The results for capillary 3 show an overreading in blood SO_2 with a reduced precision. The smallest change in blood SO_2 that could be measured in the capillary at 8.8mm depth was ±5.7%. The good agreement of the photoacoustically determined blood SO_2 with the CO-oximeter measurements is due to the fact that the blood SO_2 reflects the ratio of c_{HbO2i} and c_{THbi}, which is defined by the shape of the absorbance-related photoacoustic spectrum [5]. Blood SO_2 is therefore an inherently more robust data type than the absolute haemoglobin concentrations, which are susceptible to errors in the signal amplitude.

The analysis of the detected spectra also determined the extravascular haemoglobin concentration, c_{THbev}. The true c_{THbev} ranged between 3.7 and 4.1 g l^{-1}. The accuracy and precision in the photoacoustically determined c_{THbev} was +1.0 g l^{-1} and ±0.9 g l^{-1}, respectively. The overestimation of c_{THbev} is again presumed to be due to limitations in the forward model. The resolution in c_{THbev} was ±0.2 g l^{-1}, which is more than an order of magnitude higher than the resolution in the intravascular c_{THbi}. This is because the determination of the concentration of a distributed extravascular chromophore can be regarded as being a more constrained inverse problem since the extravascular chromophore concentration affects the amplitudes of all the spectra detected in the phantom.

It is worth noting that the resolutions in $c_{\mathrm{THb}i}$ and $c_{\mathrm{THb}ev}$ given in Table 1 are dependent upon both the measurement error and the total number of parameters (eleven in this study) that are determined from the photoacoustic spectra. An increase in either the measurement error or the number of unknown parameters without an equivalent increase in the number of data points would reduce resolution.

5. DISCUSSION

This study has validated the use of near-infrared photoacoustic spectroscopy for the quantitative, non-invasive and spatially resolved determination of chromophore concentrations. It was found that the simultaneous analysis of photoacoustic spectra obtained from different locations within the phantom and the use of a model of the wavelength-dependent photoacoustic signal amplitude were essential to determine absolute chromophore concentrations.

The accuracy, precision and resolution of this method in determining the intravascular blood SO_2 in capillary 1 and 2 (4.5mm and 6.8mm depth) compared favourably with that of the CO-oximeter. The photoacoustic $c_{\mathrm{THb}i}$ and $c_{\mathrm{THb}ev}$ determined in capillary 1 and 2 also showed reasonable agreement with the known concentrations. The blood SO_2 and $c_{\mathrm{THb}i}$ results for capillary 3 (8.8mm depth) were generally less accurate, which may be explained by the low signal-to-noise ratios that were encountered during the measurement. In addition, limitations in the forward model may also have contributed to systematic errors in the total extra- and intravascular haemoglobin concentrations.

In summary, a method for the quantitative, non-invasive and spatially resolved determination of chromophore concentrations in tissue using photoacoustic spectroscopy has been validated. The principles of the spectroscopic analysis outlined in this paper can be combined with photoacoustic imaging to provide high resolution three-dimensional maps of blood SO_2 or chromophore concentration.

6. REFERENCES

1. J. Laufer, C. Elwell, D. Delpy, and P. Beard, "Spatially resolved blood oxygenation measurements using time-resolved photoacoustic spectroscopy," *Oxygen Transport to Tissue XXVII, Series: Advances in Experimental Medicine and Biology* **578**, 155-160 (2006).
2. W. L. Kiser, R. A. Kruger, D. Reinecke, G. Kruger, and K. D. Miller, "Thermoacoustic in vivo determination of blood oxygenation," *Photons Plus Ultrasound: Imaging and Sensing* **5320**, 1-7 (2004).
3. X. D. Wang, G. Ku, X. Y. Xie, Y. W. Wang, G. Stoica, and L. V. Wang, "Non-invasive functional photoacoustic tomography of blood oxygen saturation in the brain," *Photons Plus Ultrasound: Imaging and Sensing* **5320**, 69-76 (2004).
4. Cox, BT, Arridge, SR, Köstli, KP, and Beard, PC, "2D quantitative photoacoustic image reconstruction of absorption distributions in scattering media using a simple iterative method," *Applied Optics* **45**(8), 1866-1874 (2006).
5. J. Laufer, C. Elwell, D. Delpy, and P. Beard, "In vitro measurements of absolute blood oxygen saturation using pulsed near-infrared photoacoustic spectroscopy: accuracy and resolution," *Physics in Medicine and Biology* **50**, 4409-4428 (2005).
6. K. P. Kostli and P. C. Beard, "Two-dimensional photoacoustic imaging by use of Fourier- transform image reconstruction and a detector with an anisotropic response," *Applied Optics* **42**, 1899-1908 (2003).
7. M. Cope, "The application of near infrared spectroscopy to non invasive monitoring of cerebral oxygenation in the newborn infant," Ph.D. thesis (University College London, 1991).
8. R. L. P. van Veen, H. J. C. M. Sterenborg, A. Pifferi, A. Torricelli, E. Chikoidze, and R. Cubeddu, "Determination of visible near-IR absorption coefficients of mammalian fat using time- and spatially resolved diffuse reflectance and transmission spectroscopy," *Journal of Biomedical Optics* **10**, 054004-1-054004-6 (2005).
9. G. M. Hale and M. R. Querry, "Optical constants of water in 200nm to 200mum wavelength region," *Applied Optics* **12**, 555-563 (1973).
10. H. J. van Staveren, C. J. M. Moes, J. van Marle, S. A. Prahl, and M. J. C. van Gemert, "Light-scattering in Intralipid 10% in the wavelengthh range of 400-1100nm," *Applied Optics* **30**, 4507-4514 (1991).
11. P. C. Beard, F. Perennes, and T. N. Mills, "Transduction mechanisms of the Fabry-Perot polymer film sensing concept for wideband ultrasound detection," *IEEE Transactions on Ultrasonics Ferroelectrics and Frequency Control* **46**, 1575-1582 (1999).